Novel O,N,O-coordinated organofluoroboron probe for amyloid detection: Insight from experiment and theory

SUPPORTING INFORMATION

Agata Hajda,[a] Elizaveta F. Petrusevich,[a] Robert Zaleśny,*[,a] Borys Ośmiałowski,*[,b]
Joanna Olesiak-Bańska,*[,a]

[a] *Faculty of Chemistry, Wroclaw University of Science and Technology, Wybrzeże Wyspiańskiego 27, 50-370 Wrocław, Poland*
[b] *Faculty of Chemistry, University of Gdańsk, Fahrenheit Union of Universities in Gdańsk, Wita Stwosza 63, 80-308 Gdańsk, Poland*
[c] *Faculty of Chemistry, Nicolaus Copernicus University, Gagarina 7, PL-87100 Toruń, Poland*
*E-mail: *robert.zalesny@pwr.edu.pl (R.Z.), borys.osmialowski@umk.pl (B.O.), joanna.olesiak-banska@pwr.edu.pl (J.O.-B.)*

The ester, namely ethyl (2E,4E)-5-(4-(dimethylamino)phenyl)penta-2,4-dienoate, introducing two double bonds and 1,4-phenylene as a conjugated spacer between donor and acceptor was obtained as described elsewhere.[1] The synthesis of amide and dye **2** was guided as described in previous publication by some of authors of the current manuscript.[2] The NMR spectra were recorded in DMSO-d_6 for amide used in the synthesis of **2** or $CDCl_3$, for **2**, as solvents. The dye **1** was previously described elsewhere.[3]

Amide (N-(6-(1E,3E)-4-[p-(Dimethylamino)phenyl]-1,3-butadienylcarbonylamino-2-pyridyl)-(2E,4E)-5-[p-(dimethylamino)phenyl]-2,4-pentadienamide):

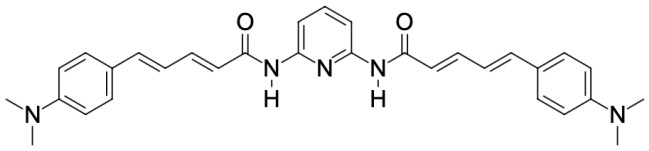

^{1}H (400 MHz, DMSO-d_6, TMS), 10.15 (s, 2H), 7.88 (d, 2H, J=7.98 Hz), 7.75 (m, 1H), 7.43 (d, 4H, J=8.9 Hz), 7.38 (dd, 2H, overlapped), 6.95 (d, 2H, J=15.4 Hz), 6.83 (dd, 2H, J=15.4, 10.9 Hz), 6.71 (d, 4H, J=8.9 Hz), 6.45 (d, 2H, J=14.9 Hz), 2.96 (s, 12H). ^{13}C (100 MHz, DMSO-d_6, TMS) 165.2, 151.2, 143.2, 141.1, 140.2, 130.9, 129.0, 124.3, 122.2, 122.1, 112.5, 112.4, 109.6, 40.25 (overlapped with solvent). HRMS 506.2558, cal. ($C_{31}H_{32}N_5O_2$) 506.2556.

Dye **2** (p-[(1E,3E)-4-[(2Z,7Z)-3-(1E,3E)-4-[p-(Dimethylamino)phenyl]-1,3-butadienyl-5-fluoro-4λ2-fluora-6-oxa-2,8,13-triaza-5-borabicyclo[7.3.1]trideca-1(13),2,7,9,11-pentaen-7-yl]-1,3-butadienyl](dimethylamino)benzene):

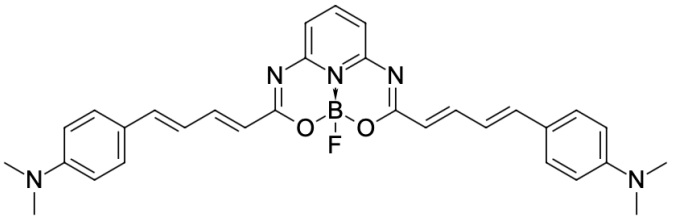

^{1}H (400 MHz, $CDCl_3$, TMS), 7.92 (t, 1H, J=8.2 Hz), 7.80 (dd, 2H, J= 14.9, 11.1 Hz), 7.44 (d, 4H, J = 8.9 Hz), 7.09 (d, 2H, J=8.0 Hz), 6.98 (d, 2H, J=15.2 Hz), 6.86 (dd, 2H, J=15.2, 11.1 Hz), 6.75 (broadened d, 4H, J=8.5 Hz), 6.26 (d, 2H, J=14.9 Hz), 3.06 (s, 12H). ^{11}B 0.53 (d, J=33 Hz). ^{13}C (150 MHz, $CDCl_3$, TMS), 166.1, 151.1, 150.4, 146.1, 144.3, 142.0, 129.0, 124.3, 122.5, 122.0, 115.8, 112.1, 40.2. HRMS 536.2646, cal. ($C_{31}H_{32}BN_5O_2F$) 536.2633.

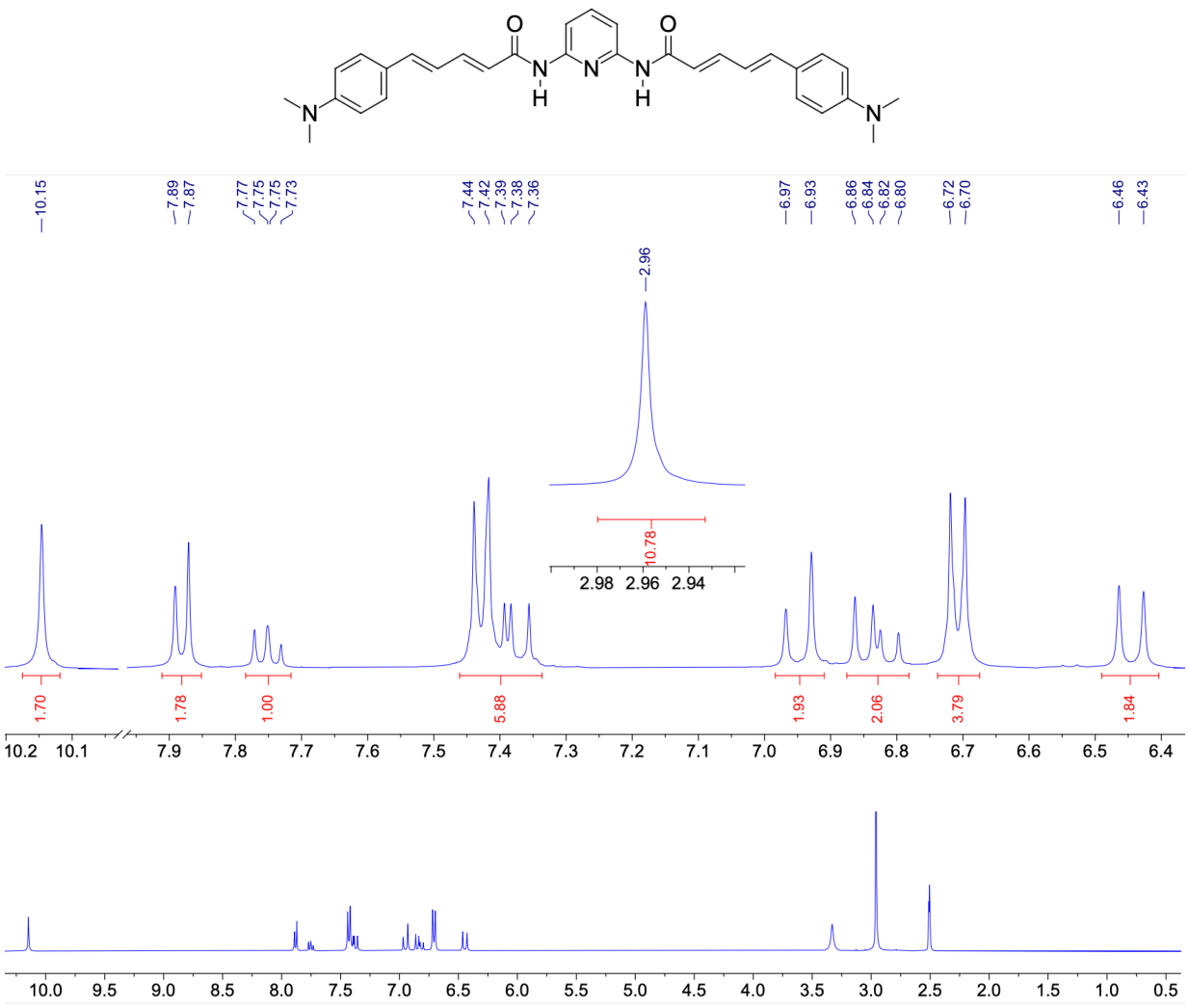

Figure S1: ^{1}H NMR spectrum (in DMSO-d_6) of amide used in the synthesis of **2**

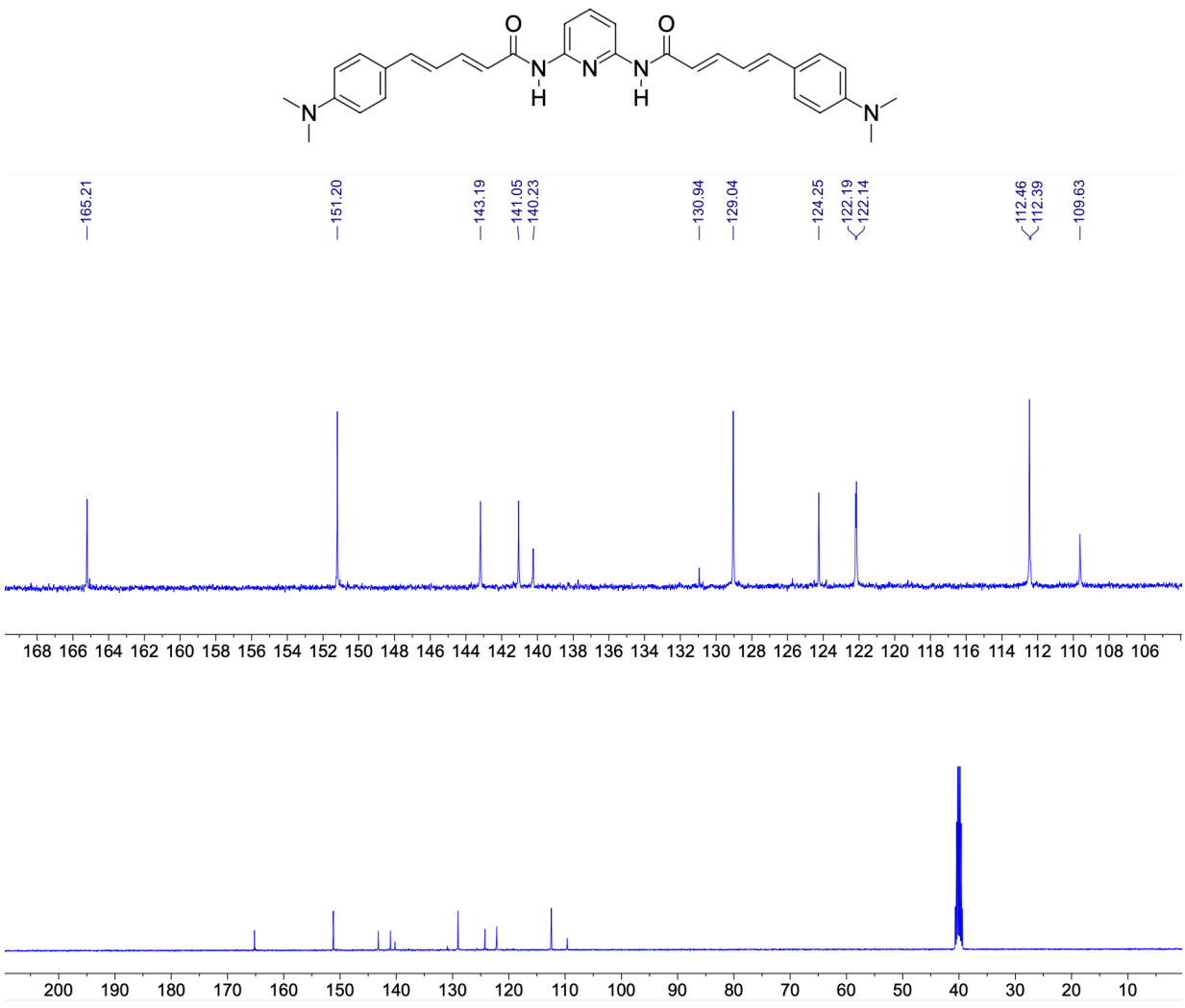

Figure S2: ^{13}C NMR spectrum (DMSO-d_6) of amide used in the synthesis of **2**

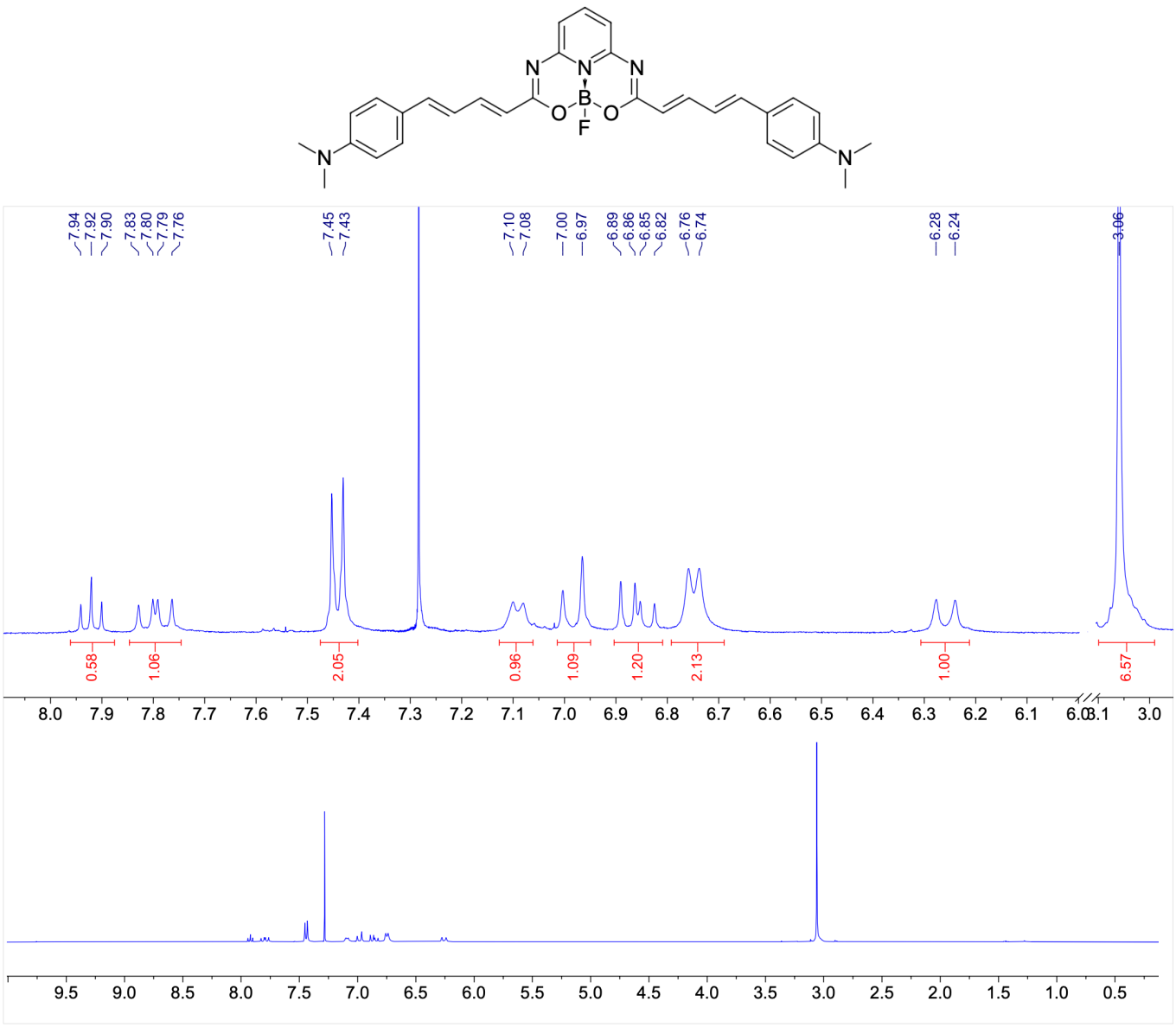

Figure S3: ^{1}H NMR spectrum (in $CDCl_3$) of **2**

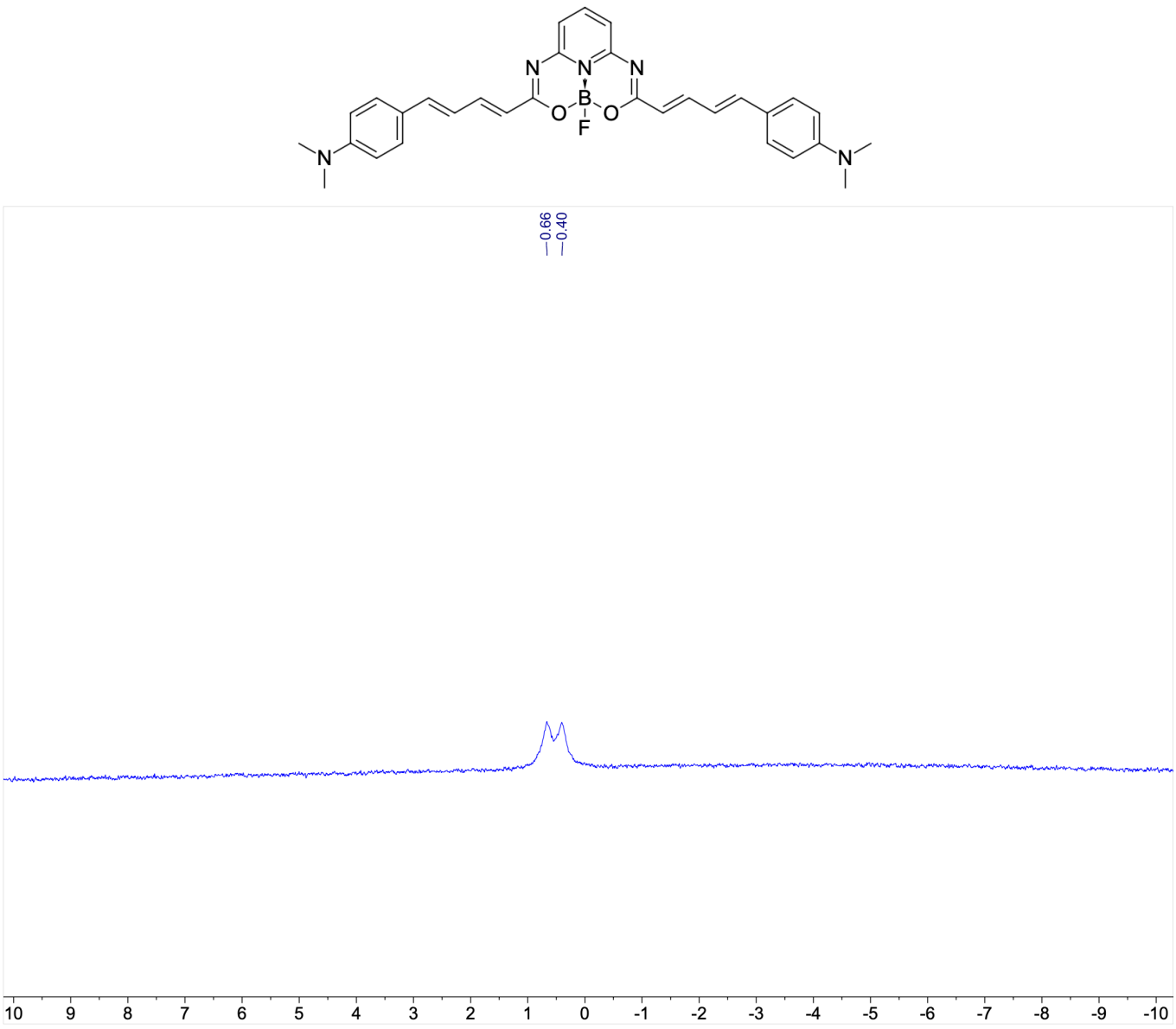

Figure S4: ^{11}B NMR spectrum (in $CDCl_3$) of **2**

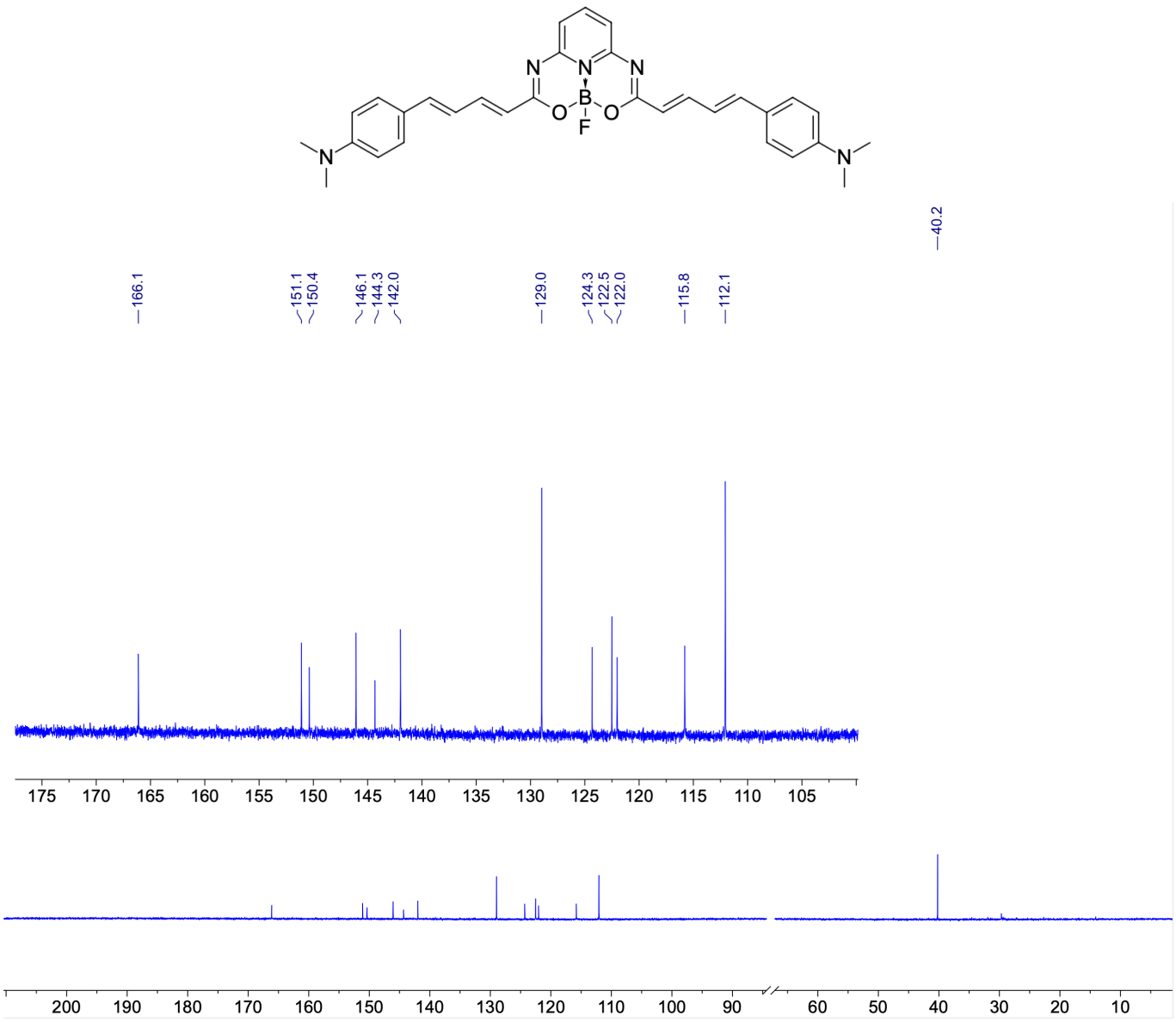

Figure S5: ^{13}C NMR spectrum (in $CDCl_3$) of **2**

One-photon measurements

Absorption spectra were recorded using a Jasco V-670 spectrophotometer, while excitation and fluorescence spectra using an FS5 Spectrofluorometer (Edinburgh Instruments) equipped with a Xenon lamp. Fluorescence lifetimes were measured using time-correlated single-photon counting technique using the same FS5 spectrometer. Samples were excited at 510 nm using a laser diode, while fluorescence decays were fitter using FAST software (Edinburgh Instruments). Chloroform for one-photon measurements was spectral grade.

Two-photon measurements

Two-photon excited photoluminescence (2PEL) was measured using a custom-built multiphoton setup. The excitation source was femtosecond mode-locked Ti:Sapphire laser (100 fs, 80 MHz, Chameleon, Coherent Inc.) with a wavelength range 680 to 1080 nm. The emission spectra were measured with a spectrograph - Shamrock 303i (Andor) with an iDUS camera (Andor). Optical filters were also used: FELH0800 - ϕ 25.0 mm Longpass Filter (Thorlabs). Stability of laser power was checked for all experimental time by power-meter (Thorlabs). The sample and reference dye were always measured at the same excitation power. 2PA cross-sections were calculated with the following equation:

$$\sigma_{2,s} = \frac{F_{2,s} C_r \phi_r n_r^2}{F_{2,r} C_s \phi_s n_s^2} \sigma_{2,r} \tag{1}$$

where r and s denote reference and sample, respectively. ϕ_r and ϕ_s is the fluorescence quantum yield. $F_{2,s}$ and $F_{2,r}$ is the integrated two-photon fluorescence intensity at a particular excitation wavelength, n is the refractive index of the solvent. C_s and C_r is the concentration of the sample and reference, respectively. LDS-698 in $CHCl_3$ was used as a reference. 2PA cross-sections of LDS-698 was obtained from previous reports.[4] FQY of LDS-698 in $CHCl_3$ was taken from Ref. 5.

Power dependence of photolumiescence intensity

To confirm the two-photon nature of the observed photoluminescence excited by laser pulses, we measured photoluminescence intensity vs incident laser excitation power and determined the power exponent, n. 2PEL was collected. For each power two spectra were collected to observed if photobleaching does not occur upon increasing laser power. The power exponent was calculated using the equation:

$$n = \frac{\log(\text{PL intensity})}{\log(\text{P})} \tag{2}$$

where PL intensity is a 2PE photoluminescence intensity and P is the average incident laser power.

Incubation of bovine insulin amyloids

Bovine insulin was purchased from Sigma-Aldrich (I5500) and dissolved in HCl solution (pH $\sim$1.5), yielding the final concentration of 2 mg/mL. The samples were incubated in an Eppendorf ThermoMixer C for 48h at 45 °C, with agitation set to 500 rpm.

Characterization of amyloids on Atomic Force Microscope (AFM)

The full procedure is described elsewhere.[6] In brief, samples were 100x diluted from stock solution (2 mg/ml). The droplets of the samples were deposited on a mica layer, rinsed with Milli-Q water after 5 min, and dried. Measurements were conducted using a Veeco Dimension V AFM in tapping mode with the SuperSharpSilicon probe mounted (Manufacturer: NANOSENSORS). Analysis of height was done in Nanoscope software for over 50 fibrils. Histogram with distibution was plotted in program OriginPro 9.0.

Characterization of amyloids on Transmission Electron Microscopy (TEM)
The solution from same sample was used as for AFM imaging to provide reliable results. 2 μL solution was placed on clean standard TEM carbon on plasma cleaned copper grids (Agar Scientific) fo 30 seconds and stained with 2 μL of uranyl acetate for additional 30 seconds. The samples were studied using Talos F200i transmission electron microscope (Thermofisher Scientific) at 200 kV accelerating voltage. Analysis of sizes was done in imageJ program fo over 50 fibrils. Histogram with distibution was plotted in program OriginPro 9.0.

Preparation of dye and amyloid samples for optical measurements (one- and two-photon)
One-photon absorption spectra were measured with a Jasco V-670 spectrophotometer in quartz cuvettes within the range of 280–700 nm. Stock solutions of dyes were prepared by dissolution in DMSO (500 μM for dye **1** and **2**; 200 μM for MeOX-4), and all solutions were prepared before use. Then, the appropriate volume of the stock solution was withdrawn and diluted so the volume of DMSO was 5% in final volume. Then appropriate amount of amyloids solution were added.

Fluorescence quantum yield of dyes
The FQY was measured by using the SC-30 Integrating Sphere Module for an FS5 spectrofluorometer from Edinburgh Instruments. **For dyes with amyloids:** The concentration of dyes was set to obtain a high signal on a two-photon microscope, as the FQY is used to calculate the 2PA cross section. The final concentration of dyes was 1 μM, and amyloid 50 μM in 5% of DMSO. Reference solution for integrating sphere was 50 μM of amyloids in 5% DMSO, to provide the same scattering.

Selectivity studies
Measurements of fluorescence changes of dye **2** (1 μM) upon binding to bioanalytes (100 μM) were measured on a clarioSTAR Plus plate reader in a 96-well black plate. Fluorescence spectra were measured 30 min after the incubation of dyes with biomolecules at 37^{o} C. To compare changes before and after binding, the fluorescence intensity (F.I) at maximum wavelength before and after binding in the same solvent were divided by each other (FI after binding / FI dye alone).

Saturation binding assay
To a solution of dye **2** the solution of insulin amyloids was added and incubated for 30 min at 37 °C. The binding solutions were measured in quartz cuvette on FS5 Spectrofluorometer (Edinburgh Instruments). For each concentration was tested in triplicate. Mean value with standard deviation was calculated and Michaelis-Menten curve was fitted in OrginPro 9.0.

Table S1: FQY of dye **2** in solvents and bovine amyloid solution (50 µM).

solvent	FQY [%]
$CHCl_3$	22
DMSO	0.6
Amyloids	10

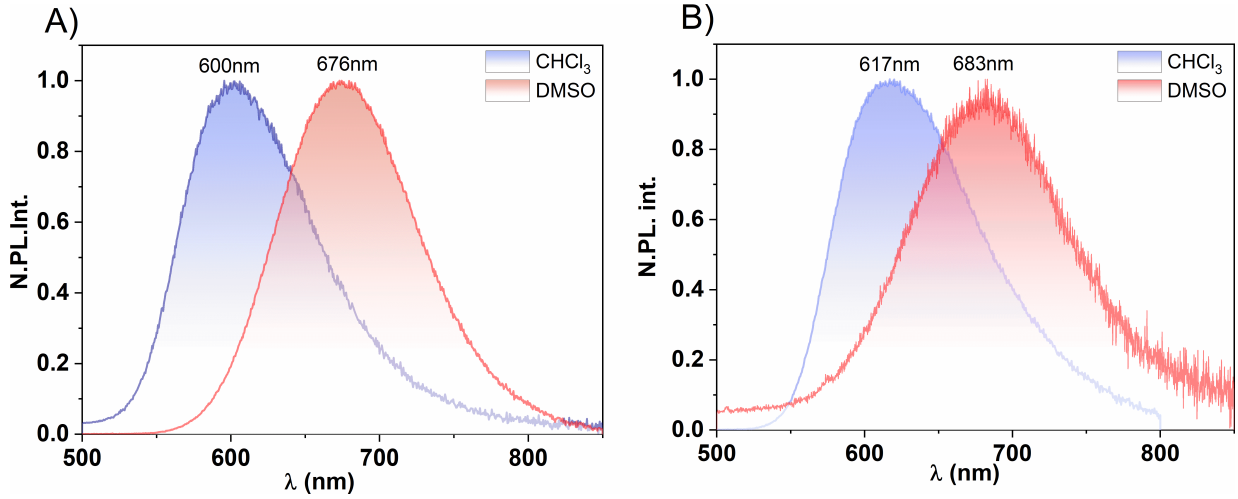

Figure S6: Normalized photoluminescence intensity (N. PL.Int.) in DMSO and $CHCl_3$ (A) dye **1** (B) dye **2**.

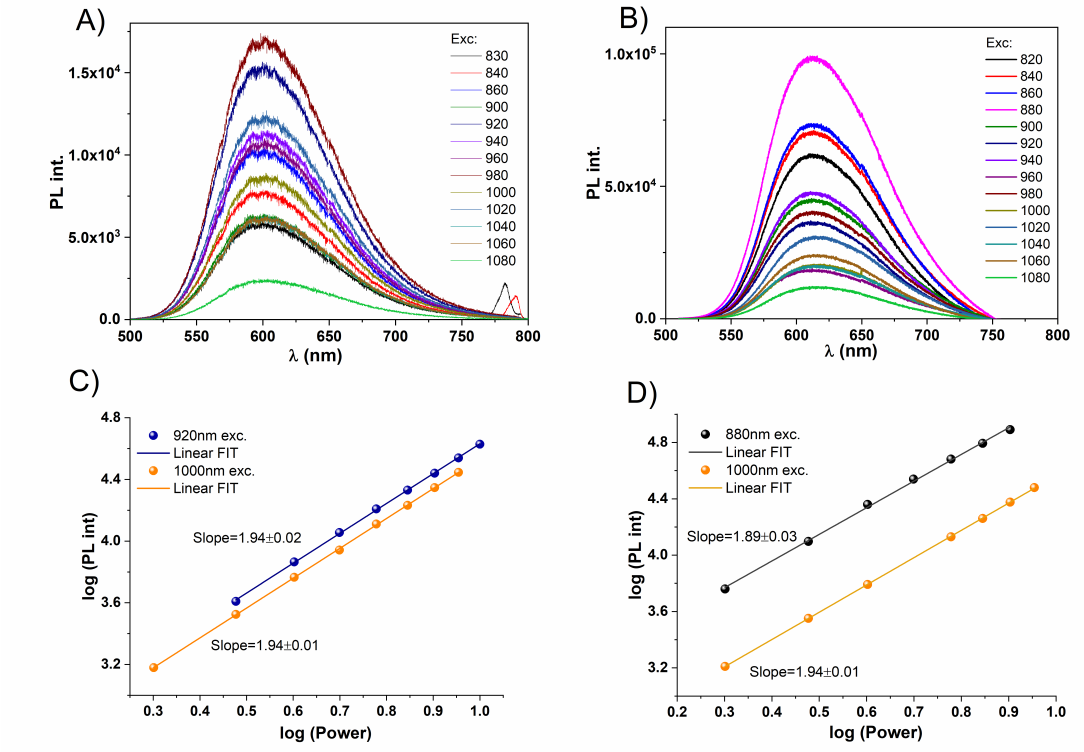

Figure S7: Two-photon excited luminescence in $CHCl_3$ of (A) dye **1** (B) dye **2**. Plots C i D shows photoluminescence intensity (PL int.) dependence on laser power for (C) dye **1** (D) dye **2**.

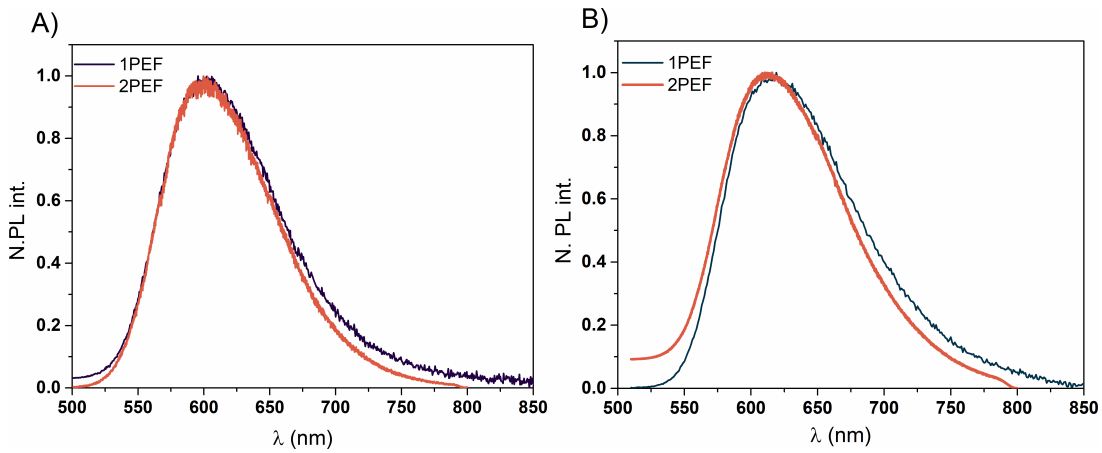

Figure S8: Normalized photoluminescence intensity (N. PL.Int.). Comparison of one-photon excited fluorescence (1PEF) vs two-photon excited fluorescence (2PEF) (A) dye **1** (B) dye **2**.

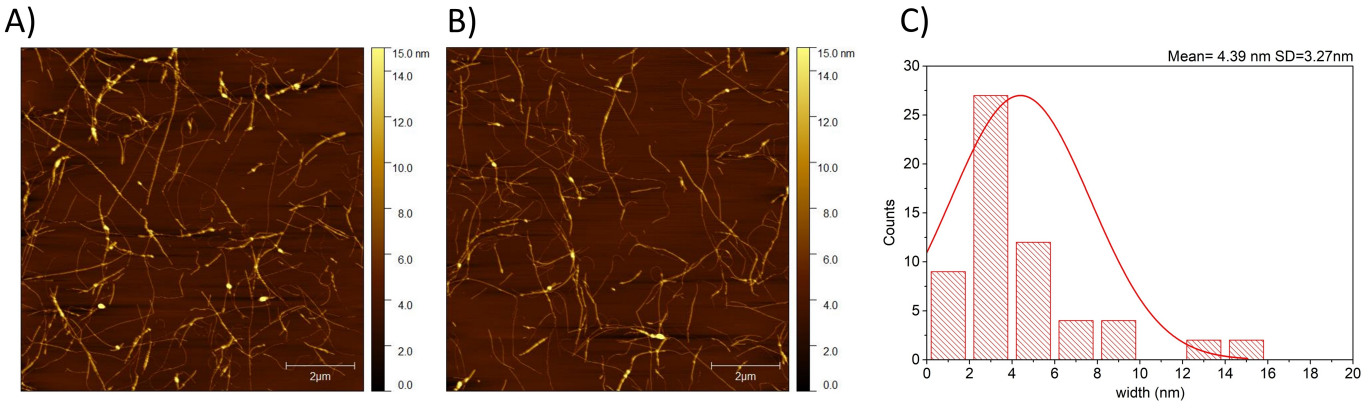

Figure S9: Atomic Forme Microscope (AFM) images of bovine insulin amyloids (A) size of scan 10x10 μm (B) size of scan 10x10 μm (C) Histogram with normal distribution of height with mean and standard deviation.

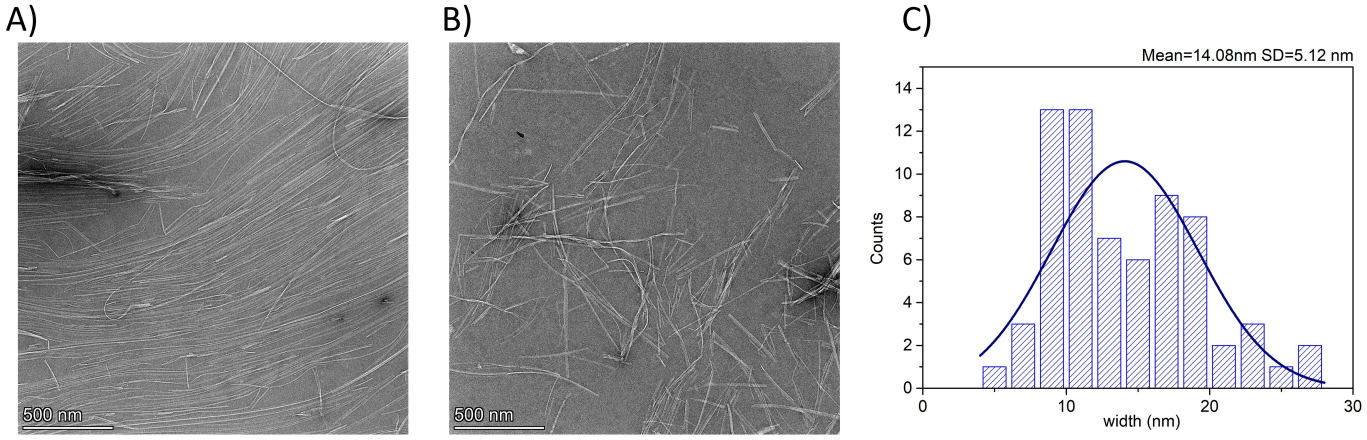

Figure S10: A) and B) TEM images of bovine insulin amyloids on two different places on grid, scale 500nm for both images; C) Histogram with normal distribution of width with mean and standard deviation.

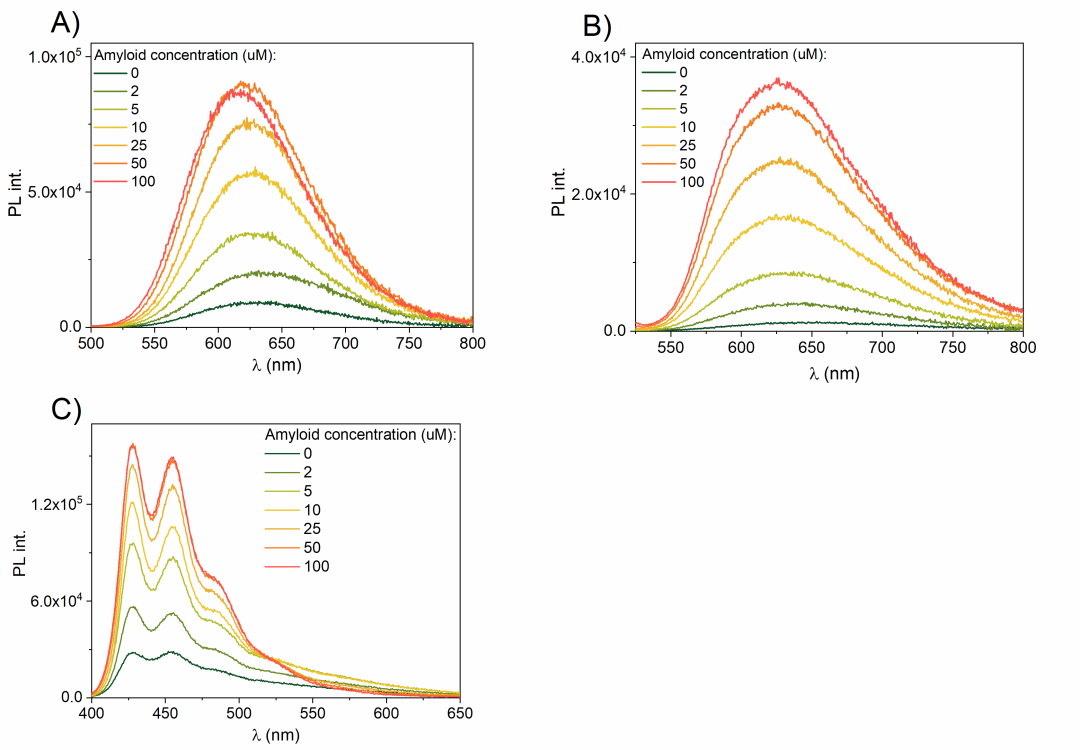

Figure S11: Spectrum of one-photon excited emission in increasing bovine insulin amyloid concentration. All solutions were 5% DMSO in water, dyes concentration was 0.5µM. (A) dye **1**; (B) dye **2** (C) MeO-X04

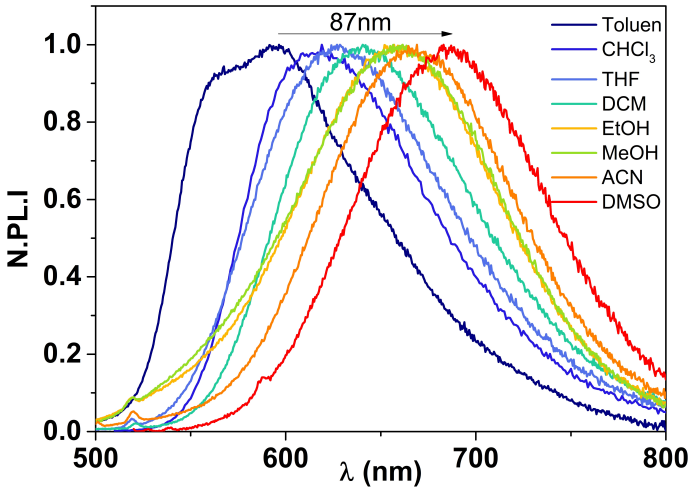

Figure S12: Emission spectrum of dye **2** in solvent with various polarity and static electric permittivity.

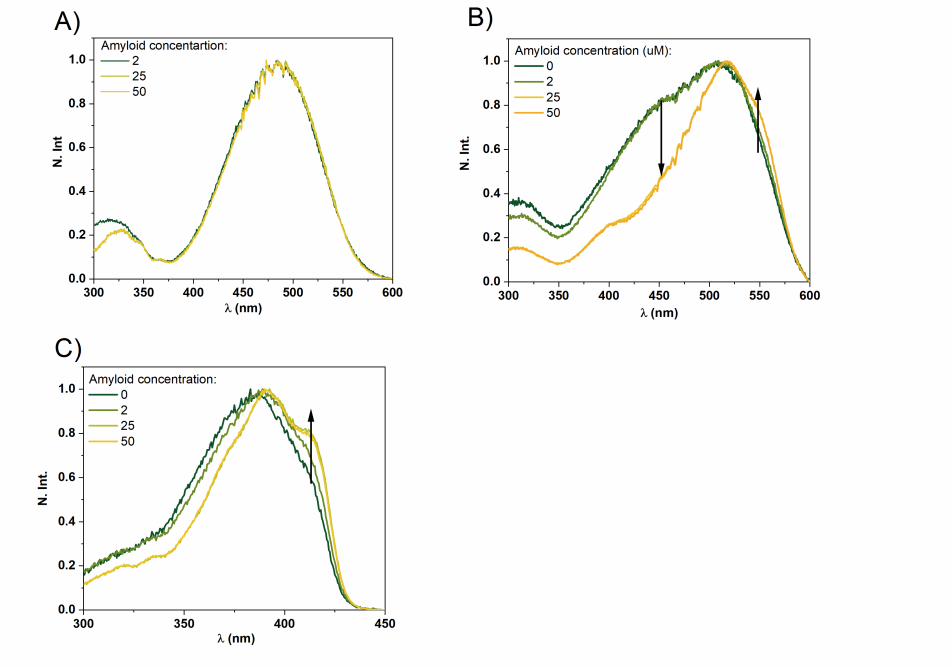

Figure S13: Spectrum of one-photon excitation in increasing bovine insulin amyloid concentration. All solutions were 5% DMSO in water, dyes concentration was 0.5µM. (A) dye **1**; (B) dye **2** (C) MeO-X04

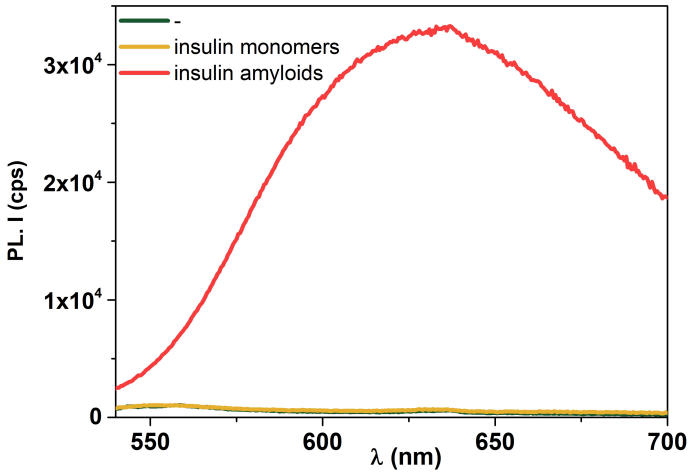

Figure S14: Emission spectrum of dye **2** only in 5% DMSO in water, upon addition of insulin monomers and insulin amyloids. Concetartion of monomers and amyloids were equal.

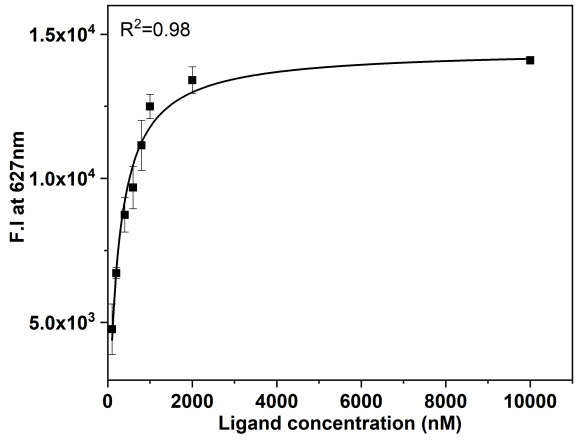

Figure S15: Saturation binding curves for ligand (dye **2)** to insulin amyloids (10 μM).

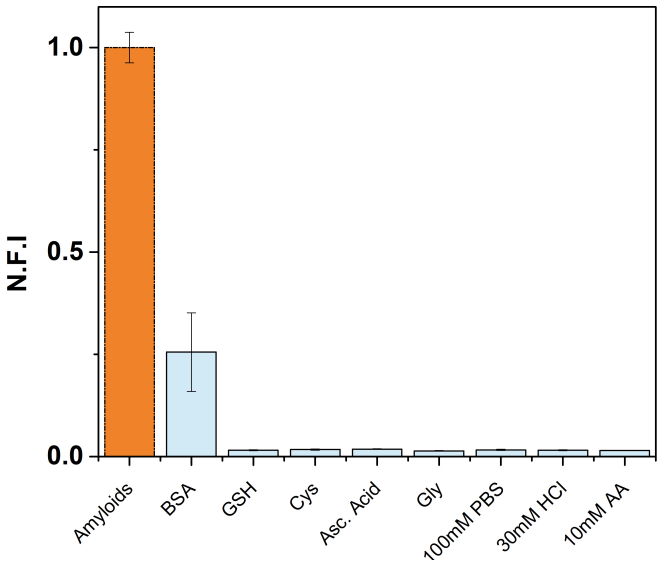

Figure S16: Selectivity studies of dye **2** (1 μM) toward potential competitive biomolecules (100 μM of Gluthation-GSH , L-cystein-Cys, Ascorbic Acid, Glycine-Gly and three different solvents: PBS pH=7.4, 10mM Ammonium Acetate pH=7.0, aqueous solution of 30mM HCl pH=1.5), different buffers and insulin aggregates (100 μM).N.F.I stands or normalized fluorescence intensity at maxima.

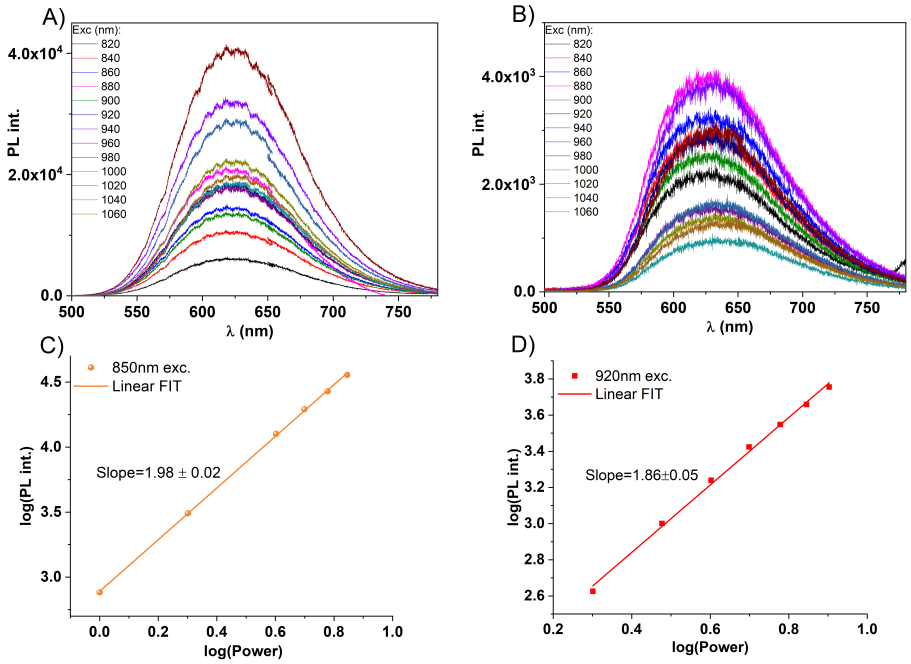

Figure S17: Two-photon excited luminescence with 50 µM of amyloids of (A) dye **1** (B) dye **2**. Plots C i D shows photoluminescence intensity (PL int.) dependence on laser power for (C) dye **1** (D) dye **2**

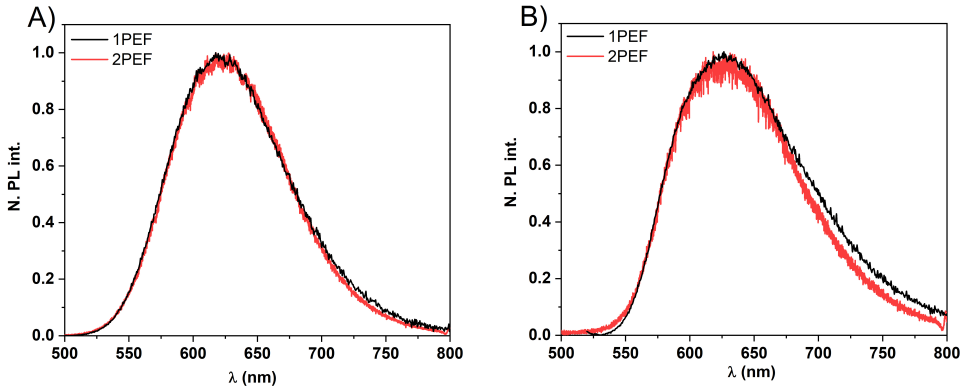

Figure S18: Normalized photoluminescence intensity (N. PL.Int.). Comparison of one-photon excited fluorescence (1PEF) vs two-photon excited fluorescence (2PEF) (A) dye **1** (B) dye **2** with 50µM of amyloids.

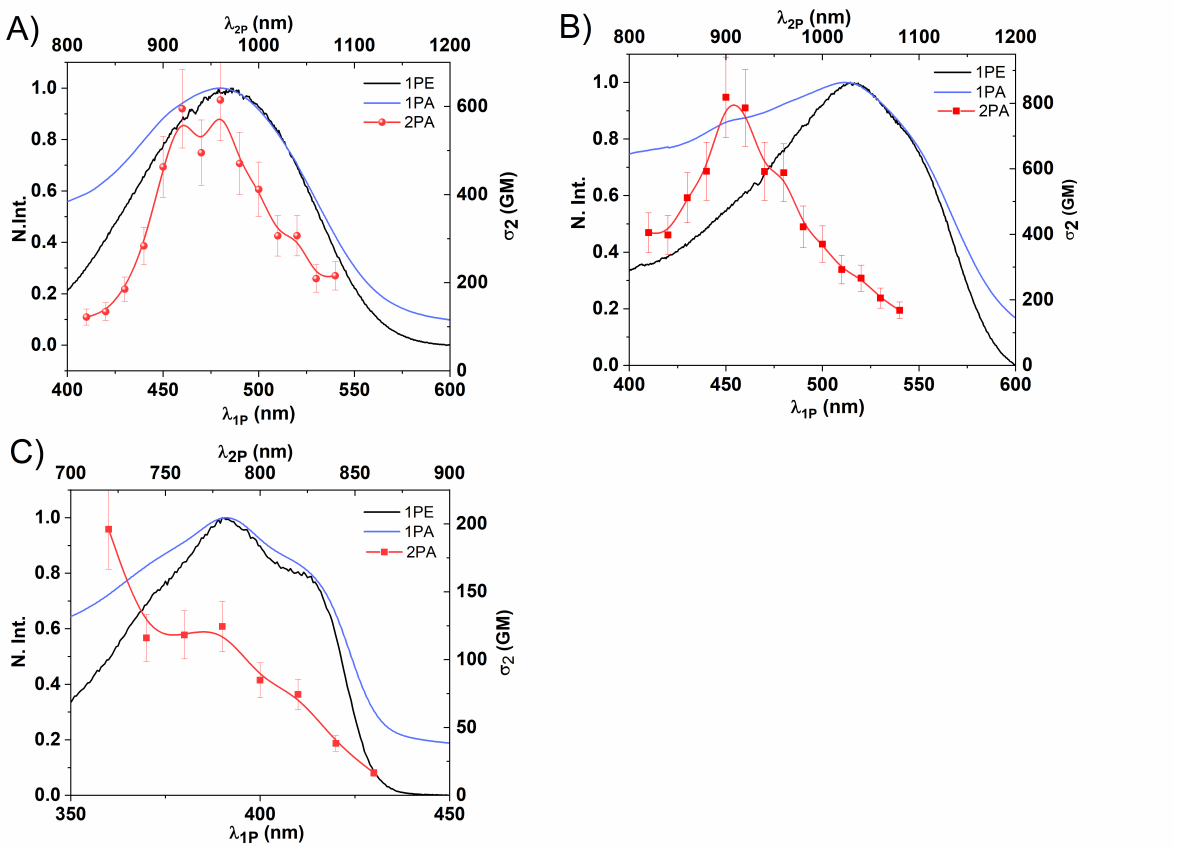

Figure S19: Experimental 2PA cross-sections compared to 1PA and 1PE of the same solution of amyloids (50 µM) with dyes (1 µM) (A) dye **1**; (B) dye **2**; (C) MeOX-04.

Two-photon absorption of dyes bound to amyloids

In our previous work we proved that 2PA can change upon interaction with protein aggregates[6] and measurements only in solvents may not give full perspective on 2PA characteristics of dyes bound to amyloid fibrils. To accurately compare two-photon and one-photon effects in dyes upon binding to amyloids, we plotted one-photon absorption (1PA), one-photon excitation (1PE) and two-photon absorption, which is represented by measured experimentally σ_2 for the same solutions (Figure S14). Normalized 1PA spectra have higher background due to scattering of amyloid solution. For dye **1** 1PA and 1PE are in line and maximum of σ_2 is around double wavelength of 1PA and 1PE. More complex story is shown in graph S14 B, which represents data for dye **2**. In 1PA peak at 515 nm dominates, however around 450 nm there is still visible peak, which is also presented in 1PA of dye **2** in $CHCl_3$ (Figure 4). In increasing amyloid concentration this peak starts to slowly vanish in 1PA. However, in the same concentration of amyloids in 1PE this peak starts to disappear more prominently, which indicates dramatic changes in one-photon radiative pathways. On the other hand 2PA has maximum around 900 nm, which corresponds to peak in one-photon regime, which decreases upon amyloid binding. It shows that 2PA of dyes maintain its shape upon binding to amyloids, as compared to measurements in $CHCl_3$, in contrast to the trend observed in 1PA and 1PE. This may be due to different selection rules for one-photon and two-photon absorption. In Figure S14 C is MeOX-4, two maxima (390, 413 nm) are present in 1PA and 1PE, which are in line with 2PA results.

Computational details

The ground state geometry optimization was performed for the studied dyes at the MN15/def2-TZVP level of theory.[7–9] Solvent environment was taken into account using the polarizable continuum model in the integral equation formalism (IEF-PCM).[10] Additionally, we confirmed that the obtained geometry corresponds to a minimum on the potential energy surface by evaluation of Hessian. In order to get insights into the electronic structure of the studied dyes, we calculated Ciofini's charge transfer diagnostic[11] and electronic density difference plots ($\Delta\rho(r) = \rho^{S_n}(r) - \rho^{S_0}(r)$) for the $S_0 \rightarrow S_1$, $S_0 \rightarrow S_2$, and $S_0 \rightarrow S_3$ transitions. The MN15/def2-TZVP/IEF-PCM level of theory was used for these analyses using Gaussian 16 program.[12]

For the further analyses of two-photon absorption we included the discrete representation of solvent environment. Studied systems were represented by the ground state geometry placed inside of the chloroform box ($50 \times 50 \times 50$ Å, 930 chloroform molecules). Molecular dynamics (MD) simulations of studied systems were performed using periodic boundary conditions. In these simulations the geometry of dye was kept rigid, while solvent molecules remained flexible. NAMD program was used to that end.[13] Subsequently, we extracted 100 "solute–solvent" snapshots per dye from the resulting MD trajectories. Approximate coupled cluster singles and doubles model using the resolution-of-identity approximation (RI-CC2)[14] and the def2-SVPP basis set[15,16] were used to simulate 2PA properties of studied systems. In these calculations electrostatic embedding model was used to include the influence of the discrete solvent environment. The described RI-CC2/def2-SVPP/EE electronic structure calculations were performed using TURBOMOLE 7.3 program.[17]

The results of RI-CC2/def2-SVPP/EE calculations for the full set of snapshots were used to determine the single snapshot (for each dye molecule) with $S_0 \rightarrow S_1$ excitation energy closest to the average over 100 solute–solvent snapshots. These two snapshots, for **1** and **2**, were subsequently used in more refined calculations at the RI-CC2/def2-TZVP/EE level of theory. In more details, we determined excitation energies, excited state dipole moments, two-photon transition strengths and all parameters required for generalized few-state model calculations.[18] These results, corresponding to RI-CC2/def2-TZVP/EE level of theory, are reported in Table 2 in the accompanying manuscript.

Two-photon absorption cross section was computed assuming Lorentzian broadening (with Γ_f equal to 0.25 eV) according to the following formula:

$$\sigma_2(\omega = \frac{1}{2}\omega_f) = \frac{8\pi^2 \alpha a_0^5 \omega^2}{c\Gamma_f} \delta^{2\mathrm{PA}} \tag{3}$$

where $\hbar\omega$ is photon energy, c is speed of light, a_0 is Bohr radius and α is fine structure constant.

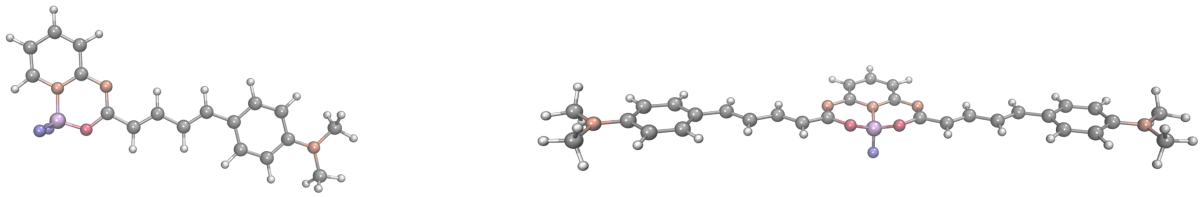

Figure S20: Ground state geometries of studied dyes determined at MN15/def2-TZVP/IEF-PCM level of theory (in chloroform). Geometry of **2** belongs to C_s symmetry point group.

Table S2: Electronic-structure parameters simulated at MN15/def2-TZVP/IEF-PCM level of theory (in chloroform): excitation energy ΔE, excitation wavelength λ, oscillator strength f, and Ciofini's charge transfer diagnostic D^{CT}.

	transition	ΔE [eV]	λ [nm]	f	D^{CT} [Å]	dominant orbital transitions
1	$S_0 \rightarrow S_1$	2.7321	453.81	1.9088	4.391	HOMO→LUMO(0.67)
	$S_0 \rightarrow S_2$	3.8919	318.57	0.0138	4.429	HOMO-1→LUMO(0.46)
	$S_0 \rightarrow S_3$	4.1362	299.75	0.1368	5.456	HOMO-1→LUMO(0.47)
						HOMO→LUMO+1(0.45)
2	$S_0 \rightarrow S_1$	2.6114	474.77	3.1577	1.085	HOMO→LUMO(0.57)
	$S_0 \rightarrow S_2$	2.8411	436.40	0.3811	1.451	HOMO-1→LUMO(0.49)
						HOMO→LUMO+1(0.48)
	$S_0 \rightarrow S_3$	3.4160	362.95	0.2733	1.122	HOMO-1→LUMO+1(0.47)

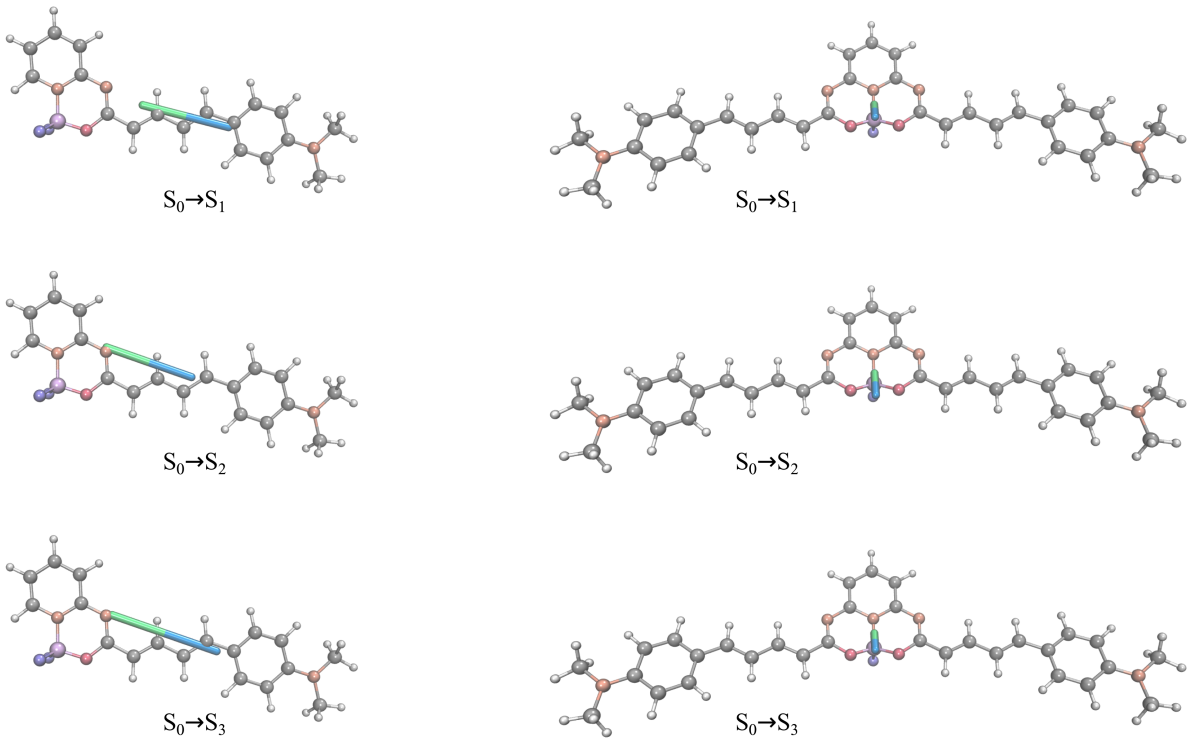

Figure S 21: Graphical representation of Ciofini's charge transfer diagnostic D^{CT} determined at MN15/def2-TZVP/IEF-PCM level of theory (in chloroform)

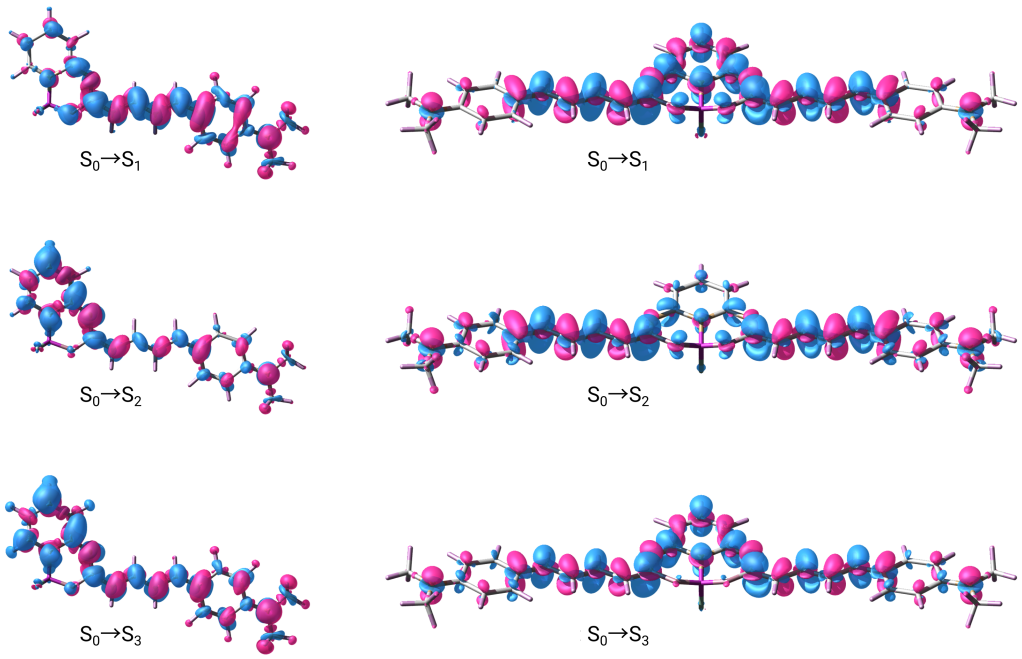

Figure S22: Electronic density difference plots corresponding to the $S_0 \rightarrow S_1$, $S_0 \rightarrow S_2$, and $S_0 \rightarrow S_3$ transitions ($\Delta\rho(r) = \rho^{S_n}(r) - \rho^{S_0}(r)$) determined at the MN15/def2-TZVP/IEF-PCM level of theory (in chloroform). Density contour value 0.001 was used.

Table S3: 1PA and 2PA properties calculated at the RI-CC2/def2-SVPP/EE level of theory (in chloroform): one-photon excitation energy ΔE, one-photon excitation wavelength λ, oscillator strength f, 2PA transition strength δ^{2PA}). In the case of each dye, the reported values correspond to a single snapshot with $S_0 \rightarrow S_1$ excitation energy closest to the average over 100 solute–solvent snapshots.

	transition	ΔE [eV]	λ [nm]	f	δ^{2PA} [a.u.]
1	$S_0 \rightarrow S_1$	3.11	399	1.85	182×10^3
	$S_0 \rightarrow S_2$	4.17	297	0.05	44×10^3
	$S_0 \rightarrow S_3$	4.43	280	0.03	21×10^3
2	$S_0 \rightarrow S_1$	2.94	421	2.99	32×10^3
	$S_0 \rightarrow S_2$	3.29	377	0.40	487×10^3
	$S_0 \rightarrow S_3$	3.68	337	0.35	37×10^3

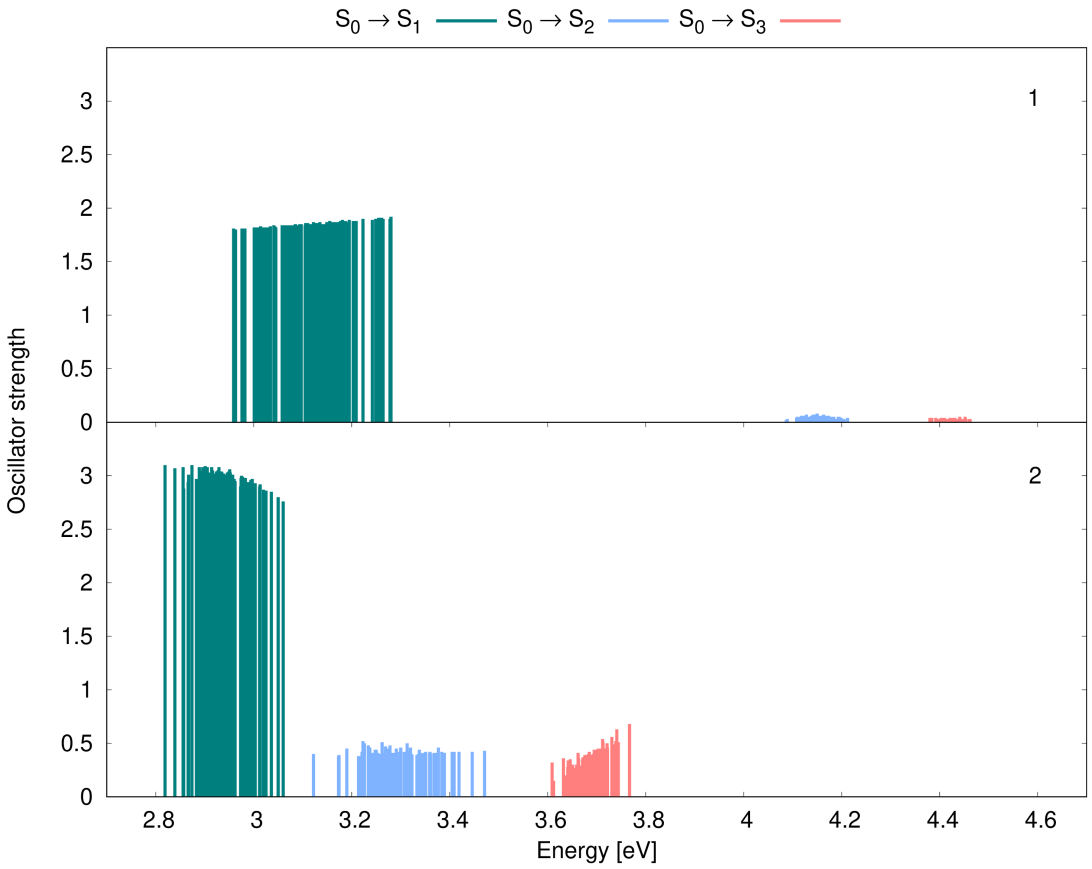

Figure S23: 1PA properties (excitation energies ΔE and oscillator strengths f) simulated for 100 snapshots at the RI-CC2/def2-SVPP/EE level of theory (in chloroform).

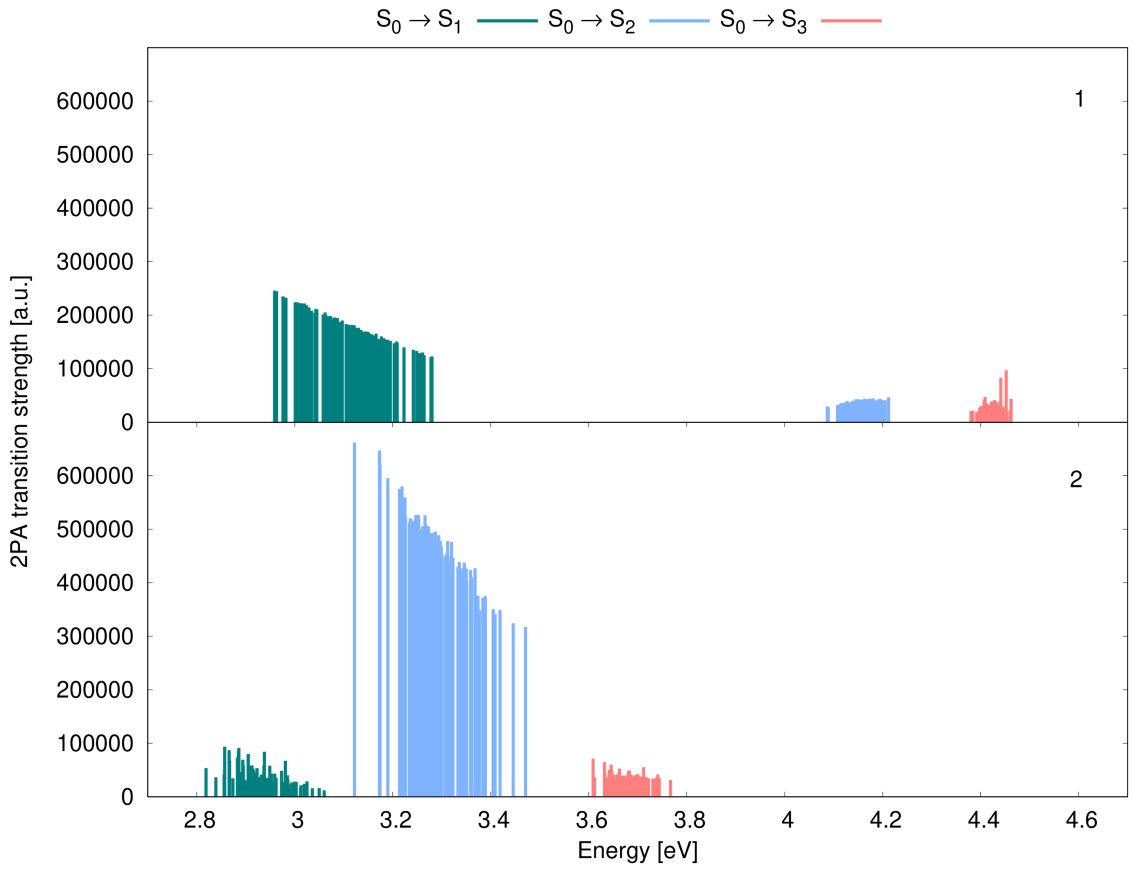

Figure S24: 2PA properties (excitation energies ΔE and 2PA transition strengths δ^{2PA}) simulated for 100 snapshots at the RI-CC2/def2-SVPP/EE level of theory (in chloroform).

References

[1] S. Iwano, R. Obata, C. Miura, M. Kiyama, K. Hama, M. Nakamura, Y. Amano, S. Kojima, T. Hirano, S. Maki and H. Niwa, *Tetrahedron*, 2013, **69**, 3847–3856.

[2] A. M. Grabarz, A. D. Laurent, B. Jędrzejewska, A. Zakrzewska, D. Jacquemin and B. Ośmiałowski, *J. Org. Chem.*, 2016, **81**, 2280–2292.

[3] B. Ośmiałowski, B. Dziuk, K. Ejsmont, L. Checińska and L. Dobrzańska, *Acta Crystallogr. C*, 2021, **77**, 807–813.

[4] N. S. Makarov, J. Campo, J. M. Hales and J. W. Perry, *Opt. Mater. Express*, 2011, **1**, 551–563.

[5] A. Hajda, R. Guha, S. M. Copp and J. Olesiak-Bańska, *Chem. Sci.*, 2025, **16**, 1737–1745.

[6] A. Hajda, M. Grelich-Mucha, P. Rybczyński, B. Ośmiałowski, R. Zaleśny and J. Olesiak-Bańska, *ACS Appl. Bio Mater.*, 2023, **6**, 5676–5684.

[7] H. S. Yu, X. He, S. L. Li and D. G. Truhlar, *Chem. Sci.*, 2016, **7**, 5032–5051.

[8] F. Weigend and R. Ahlrichs, *Phys. Chem. Chem. Phys.*, 2005, **7**, 3297–3305.

[9] F. Weigend, *Phys. Chem. Chem. Phys.*, 2006, **8**, 1057–1065.

[10] J. Tomasi, B. Mennucci and E. Cancès, *J. Mol. Struct. (Theochem)*, 1999, **464**, 211–226.

[11] T. Le Bahers, C. Adamo and I. Ciofini, *J. Chem. Theory Comput.*, 2011, **7**, 2498–2506.

[12] M. J. Frisch, G. W. Trucks, H. B. Schlegel, G. E. Scuseria, M. A. Robb, J. R. Cheeseman, G. Scalmani, V. Barone, G. A. Petersson, H. Nakatsuji, X. Li, M. Caricato, A. V. Marenich, J. Bloino, B. G. Janesko, R. Gomperts, B. Mennucci, H. P. Hratchian, J. V. Ortiz, A. F. Izmaylov, J. L. Sonnenberg, D. Williams-Young, F. Ding, F. Lipparini, F. Egidi, J. Goings, B. Peng, A. Petrone, T. Henderson, D. Ranasinghe, V. G. Zakrzewski, J. Gao, N. Rega, G. Zheng, W. Liang, M. Hada, M. Ehara, K. Toyota, R. Fukuda, J. Hasegawa, M. Ishida, T. Nakajima, Y. Honda, O. Kitao, H. Nakai, T. Vreven, K. Throssell, J. A. Montgomery, Jr., J. E. Peralta, F. Ogliaro, M. J. Bearpark, J. J. Heyd, E. N. Brothers, K. N. Kudin, V. N. Staroverov, T. A. Keith, R. Kobayashi, J. Normand, K. Raghavachari, A. P. Rendell, J. C. Burant, S. S. Iyengar, J. Tomasi, M. Cossi, J. M. Millam, M. Klene, C. Adamo, R. Cammi, J. W. Ochterski, R. L. Martin, K. Morokuma, O. Farkas, J. B. Foresman and D. J. Fox, *Gaussian 16 Revision C.01*, 2016, Gaussian Inc. Wallingford CT.

[13] J. C. Phillips, R. Braun, W. Wang, J. Gumbart, E. Tajkhorshid, E. Villa, C. Chipot, R. D. Skeel, L. Kale and K. Schulten, *J. Comput. Chem.*, 2005, **26**, 1781–1802.

[14] D. H. Friese, C. Hättig and K. Ruud, *Phys. Chem. Chem. Phys.*, 2012, **14**, 1175–1184.

[15] A. Schäfer, H. Horn and R. Ahlrichs, *J. Chem. Phys.*, 1992, **97**, 2571–2577.

[16] F. Weigend, M. Häser, H. Patzelt and R. Ahlrichs, *Chem. Phys. Lett.*, 1998, **294**, 143–152.

[17] *TURBOMOLE V7.3 2018, a development of University of Karlsruhe and Forschungszentrum Karlsruhe GmbH, 1989-2007, TURBOMOLE GmbH, since 2007; available from* `http://www.turbomole.com`.

[18] M. T. P. Beerepoot, M. M. Alam, J. Bednarska, W. Bartkowiak, K. Ruud and R. Zaleśny, *J. Chem. Theory Comput.*, 2018, **14**, 3677–3685.